Angewandte Chemie International Edition

Angewandte International Edition Chemie

GDCh German Chemical Society

How to cite: *Angew. Chem. Int. Ed.* **2026**, 65, e6661486
doi.org/10.1002/anie.6661486

COMMUNICATION OPEN ACCESS

Conformational Landscapes in the Ground and Excited States Dictate Circularly Polarized Excimer Emission: A Thermodynamic–Kinetic Interplay in Carbazole Dimer Systems

Tomohiro Kujime | Zhe Wang | Tadashi Mori

Research Center for Environmental Preservation and Department of Applied Chemistry, Graduate School of Engineering, The University of Osaka, Suita, Osaka, Japan

Correspondence: Tadashi Mori (tmori@epc.osaka-u.ac.jp)

Received: 12 March 2026 | **Revised:** 15 April 2026 | **Accepted:** 17 April 2026

Keywords: chirality | fluorescence | kinetic accessibility | luminescence dissymmetry | thermodynamic stability

ABSTRACT

We demonstrate that in chiral carbazole dimers, the *tt* conformer generates intense excimer CPL, while *gauche* rotamers yield only local emission. In **1a**, CPL intensifies and red-shifts upon cooling due to greater *tt* contribution. In contrast, the *tert*-butyl derivative **1b** shows weak, temperature-insensitive CPL owing to enhanced accessibility of non-CPL-emissive *gauche* conformers. This work reveals how subtle substituent and environmental effects modulate excited-state conformational dynamics and chiroptical responses through a thermodynamic–kinetic interplay.

1 | Introduction

Circularly polarized luminescence (CPL) from isolated small molecules—despite the intrinsic challenge of achieving large luminescence dissymmetry (g_{lum}) factors—has attracted considerable attention [1–3], particularly in helical or twisted molecular systems [4]. Among these, excimer-based CPL has recently emerged as a powerful strategy to generate chiroptical emission with enhanced g_{lum} values and tunable photophysical properties, outperforming conventional monomer-based systems [5, 6]. Pyrene-based architectures have proven especially promising and rigid scaffolds incorporating pyrene units have delivered strong excimer CPL with g_{lum} values well exceeding 0.01. For example, *trans*-1,2-di(1-pyrenylamino)cyclohexane derivatives—enabled by conformational preorganization through a rigid chiral framework—exhibit an excimer g_{lum} of 0.016 [7]. Bi- and multinaphthyl systems have demonstrated even greater efficacy, and recent studies show that judicious structural tuning combined with optimized measurement conditions can push g_{lum} values as high as 0.12 [8]. Notably, pyrene cyclophanes stand out as ideal platforms for precisely arranging pyrene chromophores in well-defined geometries, thereby amplifying CPL responses [9], while sugar-derived scaffolds such as cyclodextrins have also proven effective in this regard [10, 11]. Importantly, the CPL activity of such systems is often governed by conformation-dependent excimer formation, wherein suitable geometric variations between chromophores dramatically modulate the chiroptical response [12–14]. As a distinct example employing a different chromophore, we have demonstrated that carbazole cyclophanes afford relatively large g_{lum} values of 0.013 for partially overlapped excimer emission [15].

This amplification in the excimer arises from rigid scaffolds that preorganize chromophore pairs in close proximity, enforcing a locally twisted chiral geometry that efficiently transfers molecular chirality to the excimer state. In such systems, the emitting state is

best described as a superposition of Frenkel exciton and charge-transfer (CT) configurations, with the Frenkel component often dominating in most excimers [16]. When Frenkel interactions prevail, Davydov splitting between coupled chromophores enhances chiroptical responses through electric dipole–dipole coupling. However, strong exciton coupling alone does not guarantee excimer formation or high g_{lum} values; optimal interchromophore geometry and sufficient CT character are equally critical for efficient CPL. Within the zeroth-order approximation (neglecting minor contributions from magnetic dipole transition moments), the rotational strength R arising from the exitonic component of an excimer at frequency ν can be approximated as [17, 18]:

$$R_{\pm}\ (\text{excimer}) \propto \mp\frac{\pi\upsilon}{2}\left(\boldsymbol{R}^2-\boldsymbol{R}^1\right)\left(\boldsymbol{\mu}^1\times\boldsymbol{\mu}^2\right) \quad (1)$$

where $\boldsymbol{R}^i$ and $\boldsymbol{\mu}^i$ ($i = 1$ or 2) denote the position vectors and electric dipole transition moments of the individual chromophores, respectively. By contrast, the rotational strength for a monomeric emitter is given by:

$$R\ (\text{monomer}) \propto \text{Im}\ (\boldsymbol{\mu}\cdot\boldsymbol{m}) \quad (2)$$

where $\boldsymbol{m}$ is magnetic dipole transition moment of the emitter. Critically, excimer-based CPL typically manifests as a single, red-shifted emission band (corresponding to R_-), rather than a bisignate signal ($R_\pm$) [19]. This feature effectively bypasses the reliance on $\boldsymbol{m}$, which are intrinsically weak in organic chromophores. Beyond excimers, molecular aggregates may exhibit a similar amplification mechanism through interchromophoric coupling [20]. As such, excimer-based CPL circumvents a fundamental limitation of traditional CPL design—namely, the small magnitude of $\boldsymbol{m}$—and emerges as a versatile platform for next-generation chiroptical technologies, including 3D displays, optical data storage, and enantioselective biosensing.

While free carbazole monomers do not form intermolecular excimers under standard conditions [21], poly(vinylcarbazole) (PVCz) exhibits clear excimer emission [22]. Consequently, the photophysics of syndiotactic and isotactic PVCz has been extensively studied with model substances over the past half-century to elucidate the conformational behavior of pendant carbazole groups [23]. Classical investigations on racemic 2,4-di-*N*-carbazolylpentane, a well-established model dimer for syndiotactic PVCz, revealed that the partially overlapped "*trans–trans*" conformer is energetically favored in the ground state and directly gives rise to excimer-type emission at ~370 nm upon photoexcitation, consistent with partial π-stacking of the carbazole units [24]. Temperature- and solvent-dependent studies further highlight the contribution of non-overlapped conformers, which produce localized (monomer-like) emission near 340 nm. Although the relative populations of *trans* and *gauche* conformers in the ground state have been analyzed in detail via ^{1}H NMR coupling constants [25], the conformational landscape in the excited state, including the role of higher-energy rotamers, remains largely unexplored.

In this work, we investigate the CPL behavior of an optically pure carbazole dimer featuring two stereogenic centers that dictate both configurational and conformational preferences during excimer formation. Our combined experimental and computational analysis reveals that the conformational landscape

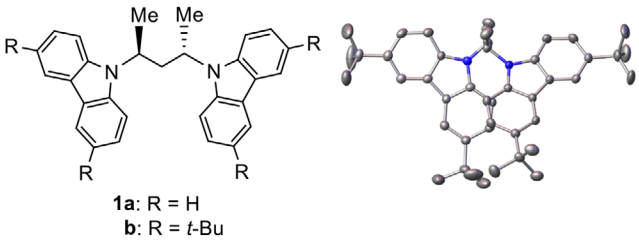

FIGURE 1 | Structures of carbazole dimers **1a** and **1b**, and x-ray crystal structure of **1b**. Details of the crystallographic analysis are provided in the Supporting Information.

about the tethering –C–CH_2–C– linkage plays a decisive role in both ground- and excited-state behavior. Moreover, the overall CPL response is governed by a dynamic interplay between (1) the ground-state conformational distribution, which is thermodynamically controlled, and (2) excited-state evolution, wherein kinetic accessibility to different conformers and their respective decay dynamics determine the observed emission profile. This synergistic control provides a refined mechanistic understanding of excimer formation and the corresponding excimer-based CPL, and opens new avenues for the rational design of chiroptical materials based on conformationally adaptive excimer systems.

2 | Results and Discussion

While the racemic form of 2,4-di(*N*-carbazolyl)pentane (**1a**) is known and has been prepared via a multi-step detour synthesis [23], we successfully prepared an enantiomerically pure sample of **1a** directly from optically pure diols (Figure 1, see Supporting Information for details). The optical purity was unequivocally confirmed by chiral HPLC (Figure S1), as well as by mirror-imaged circular dichroism (CD) and CPL spectroscopy (Figure S2). The corresponding *tert*-butyl derivative (**1b**) in optically pure form was obtained in an analogous manner. For clarity, all subsequent discussion of chiroptical properties refers to the (*S,S*)-enantiomers, which exhibit a negative CPL response.

In accordance with prior reports [23, 24], the fluorescence spectra of **1a** exhibit pronounced temperature dependence. At 25°C, the emission comprises both excimer-type fluorescence at ~370 nm and locally excited (LE) monomer-like emission, with an integrated intensity ratio of approximately 3:1 (excimer: LE). This ratio increases by nearly 100% at −110°C (Figure S3), reflecting enhanced excimer formation at low temperature. This behavior is primarily attributed to a shift in conformational equilibrium from *gauche* to *trans* conformers upon cooling. The CPL spectrum of (*S,S*)-**1a** in methylcyclohexane at 25°C displays a distinct negative signal with a g_{lum} factor of -6.6×10^{-3} at 370 nm—coincident with the excimer emission maximum in the fluorescence spectrum. In contrast, negligible CPL was observed in the region of LE (monomer-like) emission. Upon decreasing the temperature, the CPL intensity gradually increases and the emission maximum red-shifts to 380 nm at −110°C (Figure 2). Notably, this enhancement in CPL is not solely due to increased fluorescence intensity; rather, it arises from an intrinsic amplification of the chiroptical response, as evidenced by the concurrent intensification of the g_{lum} profiles with cooling ($g_{lum} = -11\times10^{-3}$ at 380 nm; see also, Figure S4). We also investigated the solvent dependence of the

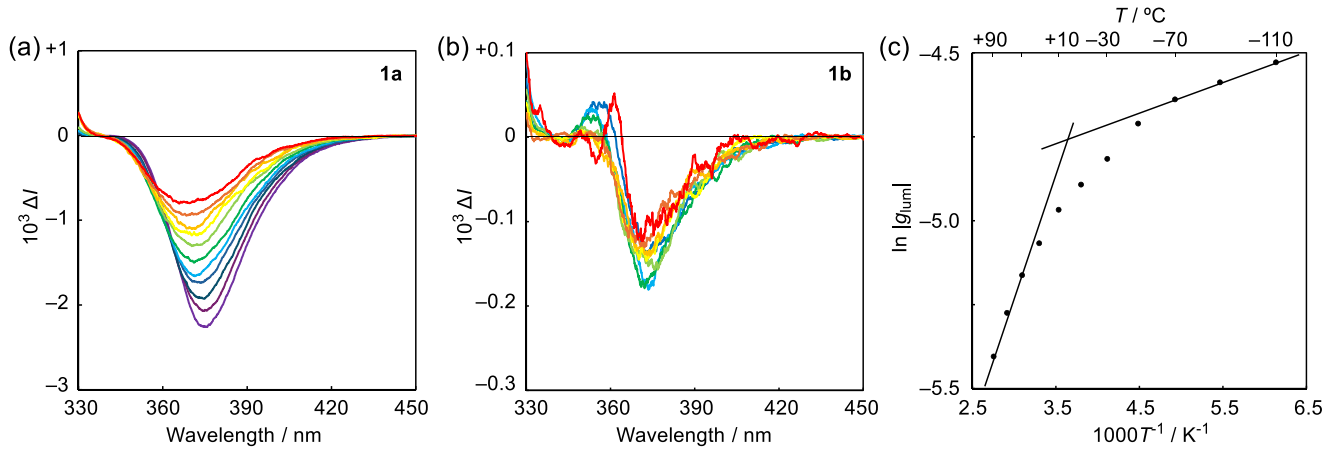

FIGURE 2 | Temperature-dependent CPL spectra of carbazole dimers (a) **1a** (+90 to −110°C) and (b) **1b** (+90°C to −50°C), and (c) the dependence of g_{lum} value of **1a** at 375 nm on reciprocal temperature ($1/T$).

CPL behavior and found it to be relatively small yet significant, reflecting the dynamic nature of conformational contributions in its excited state (Figure S5).

Although the temperature dependence of the CPL intensity of **1a** appears monotonic, the nonlinear correlation between the natural logarithm of the g_{lum} value, $\ln(|g_{lum}|)$, and reciprocal temperature ($1/T$) suggests a change in the dominant mechanism governing the CPL response. Eyring-type analysis [26] of the two apparent linear segments yields the differential apparent—and thus effective—activation enthalpy ($\Delta\Delta H^{\ddagger}_{app}$) of 6.4 kJ mol^{-1} in the high-temperature region and 0.8 kJ mol^{-1} in the low-temperature region. These effective parameters reflect the composite temperature sensitivity of the CPL response under our experimental conditions—encompassing ground-state conformational populations, excited-state relaxation pathways, and conformational interconversion dynamics—rather than a single microscopic barrier. The larger $\Delta\Delta H^{\ddagger}_{app}$ at elevated temperatures is consistent with increasing contributions from *gauche*-rich conformers that are thermodynamically disfavored in S_0 but become kinetically accessible in the flatter S_1 potential energy landscape. Temperature-dependent lifetime measurements (Figure S6) reveal a modest decrease in excimer lifetime with increasing temperature, consistent with thermally activated non-radiative decay pathways and supporting the interpretation of enhanced conformational sampling at higher temperatures. To further elucidate this behavior, we performed time-dependent density functional theory (TD-DFT) and DFT calculations on the conformational landscape of carbazole dimer **1a** in both the ground (S_0) and excited (S_1) states. A related computational study on an intermolecular carbazole dimer has been reported previously [27]. Potential energy scans were conducted as a function of the dihedral angles (ϕ_1 and ϕ_2) defined along the tethering –N–C(Me)–CH_2–C(Me)– linkage at the ωB97X-D/def2-SVP level (Figure 3). All possible conformers—combinations of *trans* (t), *gauche*$^+$ (g$^+$), and *gauche*$^-$ (g$^-$)—exhibit local minima on both the S_0 and S_1 potential energy surfaces. The partially-overlapped *tt* conformer is the global minimum, followed in energy by *tg*$^+$, *tg*$^-$, and three *gg* conformers (Figures S7 and S8). Due to high rotational barriers between conformational minima, interconversion likely occurs via single-bond rotation; concerted transformations (e.g., *tt* → *g*$^+$*g*$^+$, *g*$^+$*g*$^-$, or *g*$^-$*g*$^-$) are improbable. The *tg*$^-$ conformer lacks significant overlap between the chromophores, and its computed emission corresponds to that of a LE (monomer-like) state. In contrast, although the *tg*$^+$ conformer exhibits substantial structural overlap, calculations show it displays only local (monomer-like) emission—likely due to an unfavorable lateral offset between the chromophores combined with near-orthogonal orbital alignment, both of which suppress effective excitonic coupling and excimer formation. This assignment is corroborated by natural transition orbital (NTO) analysis, which reveals predominant hole–particle localization on a single carbazole unit (>90%) and a dipole–dipole angle ($\theta \approx 57°$) close to the magic angle for excitonic coupling, resulting in negligible dipole–dipole interaction despite geometric proximity (Figure S9). Thus, we assign the intense excimer-derived CPL exclusively to the *tt* conformer, primarily for two reasons: (1) the CPL signal is observed only in the partially overlapped excimer emission region (~380 nm), and (2) the computed rotational strengths for all other conformers are considerably smaller (vide infra). Accordingly, the TD-DFT-calculated CPL spectrum for the optimized S_1 *tt* conformer of the (*S,S*)-enantiomer—computed with the larger def2-TZVP basis set (Figure S10)—reproduces a negative signal with g_{lum} value that is slightly overestimated but in good agreement with the experiment data at low temperature, including the emission wavelength (Table 1). Such discrepancies between computed and experimental chiroptical parameters are commonly observed; the magnitude of the deviation depends on the molecular system and computational protocol [28]. Additional computational details for this and other relevant conformers are provided in Table S2.

Cooling increases the relative population of the *tt* conformer, thereby enhancing the observed CPL. This picture is consistent with studies on pyrene excimers, where time-resolved fluorescence and computation reveal that photoexcitation populates vibrationally hot Franck–Condon states on the S_1 PES, which rapidly relax toward the nearest local minimum—ultimately reaching the global minimum corresponding to a stacked, twisted geometry [29]. In **1a**, the Franck–Condon S_1 state similarly lies above the S_1 PES minimum and includes vibrational excitation. While rapid relaxation to the nearest local minimum of the same conformation occurs, the excess vibrational energy kinetically facilitates access to neighboring conformers that are

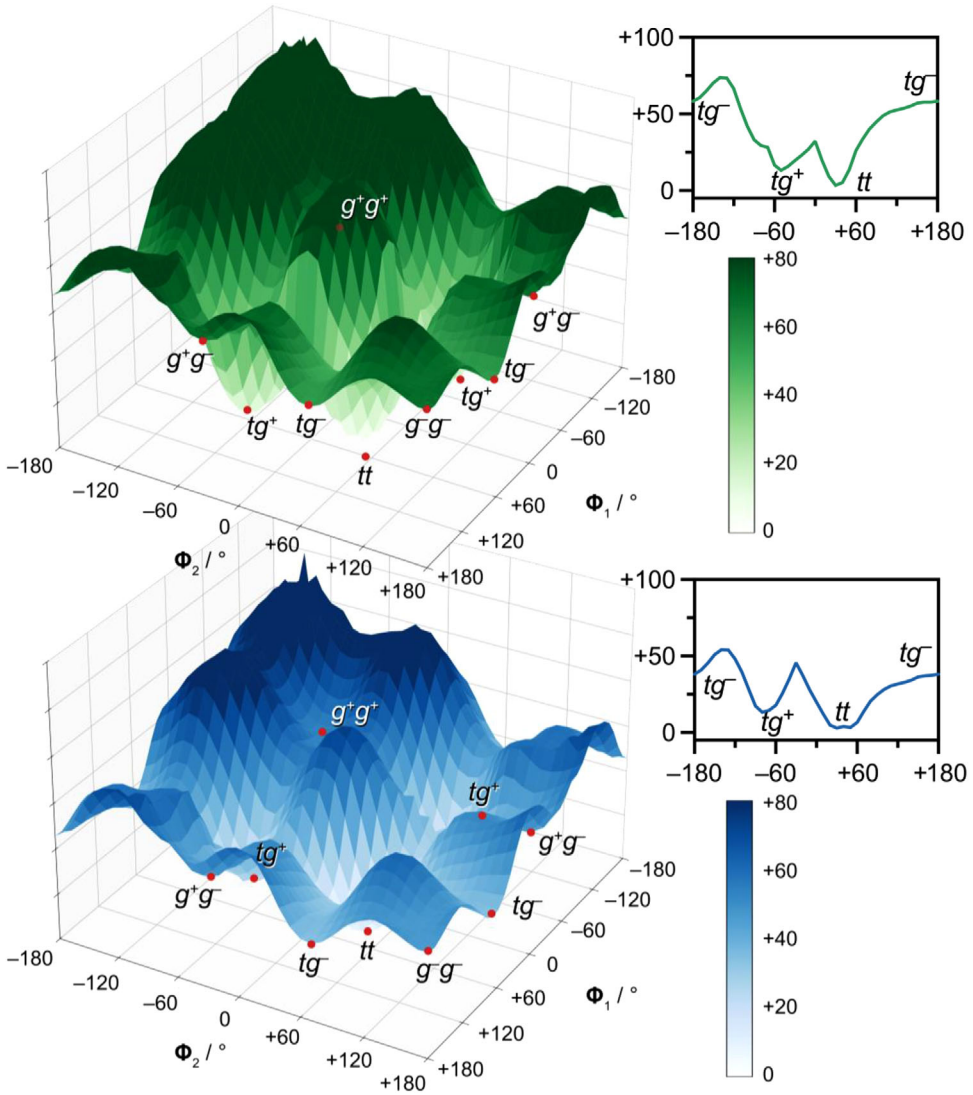

FIGURE 3 | Ground-state (S_0, bottom) and excited-state (S_1, top) potential energy hypersurfaces (PES) of carbazole dimer **1a**, mapped as a function of the dihedral angles (ϕ_1 and ϕ_2) around the tethering –C–CH_2–C– bonds, computed at the ωB97X-D/def2-SVP level. Relative energy is in kJ mol^{-1}. Insets (right) show one-dimensional PES cuts along the minimum-energy path connecting the *tt* minimum to the tg^+ and tg^- minima (with ϕ_1 fixed at 50°), illustrating the relative depths of conformational wells and the heights of intervening barriers in S_0 and S_1 states.

energetically less accessible from S_0. Indeed, the S_1 potential energy surface is significantly flatter than that of S_0, rendering conformational interconversion more facile in the excited state and directly influencing the observed CPL response (Figure 3). Consequently, at higher temperatures, greater conformational diversity—including non-emissive or weakly chiral *gauche*-rich species—leads to a blue-shifted, diminished CPL signal. The nonlinear temperature dependence of the g_{lum} value for **1a** reflects a gradual shift in the balance between thermodynamic control of the ground-state conformational distribution and kinetic factors governing excited-state conformational sampling. At low temperatures, the CPL response is dominated by the thermodynamically favored *tt* conformer; as temperature increases, enhanced population of *gauche*-rich species in S_0—coupled with facilitated excited-state interconversion on the flatter S_1 surface—progressively diminishes the excimer contribution. Such temperature- and solvent-dependent CPL arising from multi-conformer landscapes across electronic states has been already emphasized in the literature [8, 30].

Additional insight was gained from our investigation of the *tert*-butyl derivative **1b**. The crystal structure of **1b**, obtained by slow diffusion of ethanol into a toluene solution, corresponds to an alternative *tt* rotamer identified computationally as the second lowest-energy *tt* conformer. Interestingly, the most stable *tt* conformer lies 31 kJ mol^{-1} lower in energy and exhibits enhanced π-overlap between the carbazole units—a feature attributed to the dispersion-donating character of the *tert*-butyl group [31]. It has recently been emphasized that such dispersion interactions play a significant role in determining molecular structure, properties, and reactivity [32], but also in shaping excited-state behavior [33]. As previously discussed [34], the ground-state conformational distributions of **1a** and **1b** are largely comparable—both dominated by *tt* conformer—with only minor differences. This conclusion is further supported by the similarity of their CD spectra (Figure S11). In stark contrast, the fluorescence and CPL behavior of **1b** differ markedly from those of **1a**. Under identical conditions (e.g., 25°C in methylcyclohexane), the excimer contribution to the total emission in **1b** is significantly

TABLE 1 | Computed structural and spectral parameters of the *trans–trans* conformer of carbazole dimers **1a** and **1b** in the S_0 and S_1 states[(a)].

Dimer	State	ψ	d	R	D	$10^3\, g_{calc}$	$10^3\, g_{exp}$
1a	S_0	−121	4.09	−32	15 500	−8.3	−2.2
—	S_1	−112	4.19	−45	5 (400	−33	−6.6
1b[(b)]	S_0	−129	3.74	−18	19 900	−3.7	−2.7
—	—		5.52	+13	22 400	+2.2)	—
		(−129					
—	S_1	−123	4.07	−33	15 000	−8.8	−1.2
—	—		6.19	+12	38 700	+1.2)	—
		(−109					

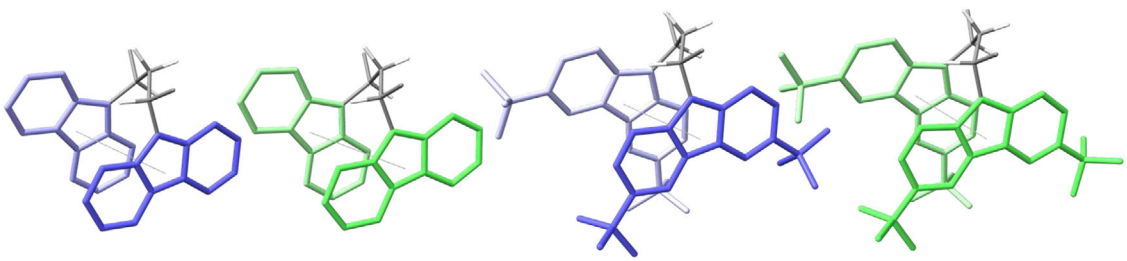

[(a)]All computations were performed at ωB97X-D/def2-TZVP level. The interplane twist angle (ψ, in degrees) and centroid-to-centroid distance (d, in Å) between carbazole units, rotational strength (R), and electric dipole strength (D) (in 10^{-40} cgs unit), and absorption or luminescence dissymmetry factors (g_{calc}) are compared. Experimental values (g_{exp}) are those obtained in methylcyclohexane at 25°C.
[(b)]Values for the second-lowest-energy local minimum structure are given in parentheses.

reduced, accounting for only ~40% of the integrated fluorescence intensity. This implies that *gauche* conformers play a more prominent role in the excited state of **1b** than in **1a**, despite their minor contribution in the ground state. Accordingly, the CPL of **1b** was significantly weaker than that of **1a**, with a g_{lum} value of -1.2×10^{-3} (Figure 2). A weak positive CPL feature near 350 nm likely originates from residual monomer-like emission of *gauche* rotamers; however, the dominant chiroptical response still stems from the excimer state. Notably, the temperature dependence is minimal; neither increasing nor decreasing the temperature substantially affected the observed CPL spectra.

Table 1 compares the optimized geometries of the partially overlapped *tt* conformers of **1a** and **1b** in both the S_0 and S_1 states. Detailed computational parameters for these and other conformers are summarized in Table S2. In both dimers, the twist (ψ) between the carbazole chromophores, defined as the dihedral angle between the long molecular axes of the carbazole units, each axis passing through the center of mass of its respective chromophore, is responsible for the strong negative chiroptical responses in both states. Upon excitation, the centroid-to-centroid distance (d) increases due to steric constraints imposed by the covalent tether—a trend opposite to that observed in untethered excimers, where excimer formation typically shortens d. Concurrently, the twist angle (ψ) increases in the excited state, enhancing excitonic coupling. This geometric reorganization results in a 2–4-fold amplification of the g_{lum} factor relative to the absorption dissymmetry (g_{abs}), consistent with Equation (1), in which ψ and d directly modulate rotational strength. A comparison of noncovalent interaction (NCI) plots [35] elucidates the origin of the structural differences between **1a** and **1b** (Figure S12). Energy decomposition analysis (Table S3) [36] reveals stronger dispersion interactions in **1b** than in **1a** mediated by the *tert*-butyl substituents, which promote closer contact and enhanced overlap of the terminal benzene rings of each carbazole unit. Consequently, **1b** in the S_1 state exhibits a slightly smaller twist angle ($\psi = -123°$ vs. $-112°$ in **1a**) but a marginally shorter interplanar distance ($d = 4.07$ Å vs. 4.19 Å). This seemingly subtle geometric difference combined with the electronic effects of the *tert*-butyl substituents, leads to a reduction in exciton-coupled CPL intensity in **1b**, arising from a combination of decreased rotational strength and increased electric dipole strength, as dictated by Equation (1).

The significantly weaker CPL response of **1b** and its relative insensitivity to temperature are also attributed to: (1) the enhanced relative stability of the tg^- conformer in **1b**, whose energy is very close to that of the *tt* conformer—in stark contrast to **1a**, where the tg^- conformer lies significantly higher in energy—and (2) a shallower energy barrier between rotamers (Figure 3). Consequently, even at low temperatures, the *tt* conformer in the S_1 state of **1b** readily relaxes into neighboring *gauche*-rich conformations. The extent of this relaxation is relatively temperature-independent, leading to the observed insensitivity of the CPL response across the measured temperature range. These results highlight that conformational contributions to chiroptical emission—governed by the interplay of thermodynamic stability (relative conformer energies) and kinetic accessibility (interconversion barriers)—are exquisitely sensitive to subtle substituent modifications in the molecular

scaffold, with particularly pronounced effects manifesting in the excited state.

3 | Conclusion

In conclusion, we have extensively investigated—through a combined experimental and computational approach—the CPL behavior of an optically pure carbazole dimer, a system long employed as a molecular model for syndiotactic PVCz. Our study underscores the critical role of the interplay between thermodynamic stability and kinetic accessibility of conformers in the excited state in shaping the overall CPL response, achieved by mapping and analyzing the complete conformational landscape around the connecting propylene linkage in both the ground (S_0) and excited (S_1) states. The relative contributions of these factors are sensitively modulated by temperature, solvent environment, and substituents on the carbazole core. We are currently extending this work to diverse intra- and intermolecular excimer systems that exhibit tunable CPL signatures through structural and environmental control. Excimer-based CPL addresses a central challenge in chiroptical materials: achieving large luminescence dissymmetry (g_{lum}) factors while maintaining high photoluminescence quantum yields (Φ_{lum}) [37]. The traditionally transient and structurally ambiguous nature of excimers has been overcome through preorganized molecular architectures featuring a simple chiral linkage, which enforces predictable, well-defined chiral excimer geometries. Current efforts focus on advancing excimer CPL into functional applications, including electroluminescent devices, white-light CPL emitters, and biological imaging probes with enhanced signal-to-noise ratios for chiral sensing. We anticipate that these developments will yield significant progress in the near future.

Author Contributions

Tomohiro Kujime: data curation, writing – review, and editing. **Zhe Wang**: software, writing – review, and editing. **Tadashi Mori**: conceptualization, investigation, funding acquisition, writing – review and editing, writing – original draft, project administration, and supervision.

Acknowledgments

This work was supported by Grants-in-Aids for Scientific Research from the Japan Society for the Promotion of Science (JSPS) (Grant No. JP25K01752), the JSPS Core-to-Core Program (Grant No. JPJSCCA20250005), and the Core Research for Evolutional Science and Technology (CREST) program of the Japan Science and Technology Agency (JST) (Grant No. JPMJCR2001).

Conflicts of Interest

The authors declare no conflicts of interest.

Data Availability Statement

The data that supports the findings of this study are available in the Supporting Information of this article.

References

1. Y. Zhang, S. Yu, B. Han, et al., "Circularly Polarized Luminescence in Chiral Materials," *Matter* 5 (2022): 761–791.

2. J. R. Brandt, F. Salerno, and M. J. Fuchter, "The Added Value of Small-Molecule Chirality in Technological Applications," *Nature Reviews Chemistry* 1 (2017): 0045, https://doi.org/10.1038/s41570-017-0045.

3. G. Longhi, E. Castiglioni, J. Koshoubu, G. Mazzeo, and S. Abbate, "Circularly Polarized Luminescence: A Review of Experimental and Theoretical Aspects," *Chirality* 28 (2016): 696–707, https://doi.org/10.1002/chir.22647.

4. T. Mori, "Small Molecule Helical Emitters," *Chemical Society Reviews* 55 (2026): 1999–2023, https://doi.org/10.1039/D5CS01270H.

5. J. Zhao, S. Shi, X. Zhang, et al., "Circularly Polarized Luminescence Pyrene Materials: From Design to Applications," *Coordination Chemistry Reviews* 548 (2026): 217173, https://doi.org/10.1016/j.ccr.2025.217173.

6. Y. Ohishi and M. Inouye, "Circularly Polarized Luminescence From Pyrene Excimers," *Tetrahedron Letters* 60 (2019): 151232, https://doi.org/10.1016/j.tetlet.2019.151232.

7. M. J. Álvaro-Martins, C. Billiaux, P. Godard, R. Oda, G. Raffy, and D. M. Bassani, "Strong Circularly Polarized Luminescence via Intramolecular Excited-State Symmetry-Breaking Charge Separation," *Chemical Communications* 59 (2023): 922–929.

8. K. Takaishi, Y. Sato, and T. Ema, "Quadruply Bridging Strategy Intensifies Circularly Polarized Luminescence of Azapyrenophanes," *Journal of the American Chemical Society* 148 (2026): 5923–5929, https://doi.org/10.1021/jacs.5c22797.

9. L.-T. Bao, R.-H. Zhang, X. Yuan, et al., "Rigidly Locked Pyrene Excimers in Planar Chiral Pyrenophanes for Intense and Stable Circularly Polarized Photoluminescence and Electrochemiluminescence," *Angewandte Chemie International Edition* 64 (2025): e202500472, https://doi.org/10.1002/anie.202500472.

10. H. Shigemitsu, K. Kawakami, Y. Nagata, et al., "Cyclodextrins With Multiple Pyrenyl Groups: An Approach to Organic Molecules Exhibiting Bright Excimer Circularly Polarized Luminescence," *Angewandte Chemie International Edition* 61 (2022): e202114700, https://doi.org/10.1002/anie.202114700.

11. C. Tu, W. Wu, W. Liang, et al., "Host–Guest Complexation-Induced Aggregation Based on Pyrene-Modified Cyclodextrins for Improved Electronic Circular Dichroism and Circularly Polarized Luminescence," *Angewandte Chemie International Edition* 61 (2022): e202203541, https://doi.org/10.1002/anie.202203541.

12. X. Li, W.-T. Xu, X.-Q. Xu, et al., "Lighting Up Bispyrene-Functionalized Chiral Molecular Muscles With Switchable Circularly Polarized Excimer Emissions," *Angewandte Chemie International Edition* 64 (2025): e202412548, https://doi.org/10.1002/anie.202412548.

13. G. Bella, M. Milone, G. Bruno, and A. Santoro, "Triphasic Circularly Polarized Luminescence Switch Quantum Simulation of a Topologically Chiral Catenane," *Journal of Materials Chemistry C* 12 (2024): 3005–3012, https://doi.org/10.1039/D3TC04491B.

14. V. Zullo, A. Iuliano, G. Pescitelli, and F. Zinna, "Tunable Excimer Circularly Polarized Luminescence in Isohexide Derivatives From Renewable Resources," *Chemistry—A European Journal* 28 (2022): e202104226, https://doi.org/10.1002/chem.202104226.

15. K. Tani, R. Imafuku, K. Miyanaga, et al., "Combined Experimental and Theoretical Studies on Planar Chirality of Partially Overlapped C_2-Symmetric [3.3](3,9)Dicarbazolophanes," *Journal of Physical Chemistry A* 124 (2020): 2057–2063, https://doi.org/10.1021/acs.jpca.0c00286.

16. Y. J. Bae, D. Shimizu, J. D. Schultz, et al., "Balancing Charge Transfer and Frenkel Exciton Coupling Leads to Excimer Formation in Molecular Dimers: Implications for Singlet Fission," *Journal of Physical Chemistry A* 124 (2020): 8478–8487, https://doi.org/10.1021/acs.jpca.0c07646.

17. G. Pescitelli, "ECD Exciton Chirality Method Today: A Modern Tool for Determining Absolute Configurations," *Chirality* 34 (2022): 333–363, https://doi.org/10.1002/chir.23393.

18. N. Harada and K. Nakanishi, "Exciton Chirality Method and Its Application to Configurational and Conformational Studies of Natural

Products," *Accounts of Chemical Research* 5 (1972): 257–263, https://doi.org/10.1021/ar50056a001.

19. J. L. Greenfield, J. Wade, J. R. Brandt, X. Shi, T. J. Penfold, and M. J. Fuchter, "Pathways to Increase the Dissymmetry in the Interaction of Chiral Light and Chiral Molecules," *Chemical Science* 12 (2021): 8589–8602, https://doi.org/10.1039/D1SC02335G.

20. Y. Yang, C. Yang, X. Zhu, L. Zhang, and M. Liu, "Interfacial Self-Assembly of a Chiral Pyrene Exciplex Into a Superhelix With Enhanced Circularly Polarized Luminescence," *Chemical Communications* 60 (2024): 6631–6634, https://doi.org/10.1039/D4CC01820F.

21. K. Lee and D. Kim, "A Theoretical Study of Carbazole Dimers: Does Carbazole Form an Excimer That Undermines the Performance of Organic Light Emitting Diodes?" *International Journal of Quantum Chemistry* 120 (2020): e26363, https://doi.org/10.1002/qua.26363.

22. M. Yokoyama, T. Tamamura, M. Atsumi, M. Yoshimura, Y. Shirota, and H. Mikawa, "Excimer Formation by Poly(*N*-Vinylcarbazole) in Solution," *Macromolecules* 8 (1975): 101–104, https://doi.org/10.1021/ma60044a002.

23. F. Evers, K. Kobs, R. Memming, and D. R. Terrell, "Intramolecular Excimer Emission of Poly(*N*-Vinylcarbazole) and *Rac*- and *Meso*-2,4-Di-*N*-Carbazolylpentane. Model Substances for Its Syndiotactic and Isotactic Dyads," *Journal of the American Chemical Society* 105 (1983): 5988–5995, https://doi.org/10.1021/ja00357a005.

24. J. Vandendriessche, P. Palmans, S. Toppet, N. Boens, F. C. De Schryver, and H. Masuhara, "Configurational and Conformational Aspects in the Excimer Formation of Bis(Carbazoles)," *Journal of the American Chemical Society* 106 (1984): 8057–8064, https://doi.org/10.1021/ja00338a009.

25. A. Abe, H. Kobayashi, T. Kawamura, M. Date, T. Uryu, and K. Matsuzaki, "Statistical Properties of the Poly(N-Vinylcarbazole) Chain as Estimated From an NMR Analysis of 2,4-Bis-*N*-Carbazolylpentane," *Macromolecules* 21 (1988): 3414–3419, https://doi.org/10.1021/ma00190a011.

26. H. Eyring, "The Activated Complex in Chemical Reactions," *Journal of Chemical Physics* 3 (1935): 107–115, https://doi.org/10.1063/1.1749604.

27. P. de Sainte Claire, "Molecular Simulation of Excimer Fluorescence in Polystyrene and Poly(Vinylcarbazole)," *Journal of Physical Chemistry B* 110 (2006): 7334–7343, https://doi.org/10.1021/jp056987e.

28. C. A. Guido, F. Zinna, and G. Pescitelli, "Quantum Chemistry Calculations of Circularly Polarized Luminescence (CPL): From Spectral Modeling to Molecular Design," *Chemical Reviews* 125 (2025): 10492–10656, https://doi.org/10.1021/acs.chemrev.5c00359.

29. G. Parolin, B. C. Garain, S. Mukherjee, G. Granucci, S. Corni, and M. Barbatti, "Conformational Dynamics of the Pyrene Excimer," *Physical Chemistry Chemical Physics* 26 (2024): 29351–29363, https://doi.org/10.1039/D4CP03947E.

30. G. Namba, Y. Mimura, Y. Imai, R. Inoue, and Y. Morisaki, "Control of Axial Chirality by Planar Chirality Based on Optically Active [2.2]Paracyclophane," *Chemistry—A European Journal* 26 (2020): 14871–14877, https://doi.org/10.1002/chem.202003188.

31. S. Rösel, H. Quanz, C. Logemann, et al., "London Dispersion Enables the Shortest Intermolecular Hydrocarbon H···H Contact," *Journal of the American Chemical Society* 139 (2017): 7428–7431.

32. M. H. J. Domanski, M. Fuhrmann, and P. R. Schreiner, "London Dispersion as a Design Element in Molecular Catalysis," *Journal of the American Chemical Society* 147 (2025): 29611–29623, https://doi.org/10.1021/jacs.5c09212.

33. K. Nagasaki, Y. Inoue, and T. Mori, "Entropy-Driven Diastereoselectivity Improvement in the Paternò-Büchi Reaction of 1-Aphthyl Aryl Ethenes With a Chiral Cyanobenzoate Through Remote Alkylation," *Angewandte Chemie International Edition* 57 (2018): 4880–4885, https://doi.org/10.1002/anie.201801330.

34. S. Ito, K. Takami, Y. Tsujii, and M. Yamamoto, "Excimer Formation in Sterically Hindered Poly(9-Vinylcarbazole) and Its Dimer Model Compounds," *Macromolecules* 23 (1990): 2666–2673, https://doi.org/10.1021/ma00212a012.

35. T. Lu, "Visualization Analysis of Covalent and Noncovalent Interactions in Real Space," *Angewandte Chemie International Edition* 64 (2025): e202504895, https://doi.org/10.1002/anie.202504895.

36. D. G. A. Smith, L. A. Burns, A. C. Simmonett, et al., "PSI4 1.4: Open-Source Software for High-Throughput Quantum Chemistry," *Journal of Chemical Physics* 152 (2020): 184108, https://doi.org/10.1063/5.0006002.

37. Y. Nagata and T. Mori, "Irreverent Nature of Dissymmetry Factor and Quantum Yield in Circularly Polarized Luminescence of Small Organic Molecules," *Frontiers in Chemistry* 8 (2020): 448, https://doi.org/10.3389/fchem.2020.00448.

38. Deposition number 2536729 (for **1b**) contains the supplementary crystallographic data and is provided free of charge by the joint Cambridge Crystallographic Data Centre (CCDC) and Fachinformationszentrum (FIZ) Karlsruhe Access Structures service.

Supporting Information

Additional supporting information can be found online in the Supporting Information section.

Supporting File 1: Experimental procedure, additional spectra, and computational details (PDF), crystal structure of **1b** (cif) [38]. The authors have cited additional references within the Supporting Information [39–49].